Pergamon

Cement and Concrete Research, Vol. 26, No. 1, pp. 125-137, 1996

0008-8846/96 $15.00 + .00

0008-8846(95)00194-8

OBSERVATION OF MIXED MODE FRACTURE WITH CENTER NOTCHED DISK SPECIMENS

Z. Jia, A. Castro-Montero and S.P. Shah
Northwestern University, Evanston, Illinois 60208

(Refereed)
(Received January 16; in final form October 23, 1995)

ABSTRACT

Center notched disk (CND) specimens were loaded diametrically under Brazilian test configuration. By changing the notch inclination angle with respect to the loading direction the mode of fracture was varied from mode I (tensile) to mixed mode (tension-shear and compression-shear). The tests were conducted at two rates of loading. First, a quasi-static rate of loading was used under closed loop testing conditions. High rate of loading was applied using an instrumented Charpy machine. The selected impact rate of loading did not modify the failure mode. Failure was still the result of propagation of a single crack. At quasi-static rate, both laser holographic interferometry and reflection photoelasticity with conventional TV imaging were used to observe mixed mode fracture in the center notched disk specimens. Reflection photoelasticity and high speed photography were used to monitor the crack growth at impact rate. Laser holographic interferometry was also used to calibrate reflection photoelasticity recordings on similar specimens at comparable rates of loading. For all notch inclination angles, the peak load increased by a constant factor relative to the peak loads at quasi-static rate of loading. However, the increase of apparent stress intensity factor at crack initiation for tensile cracking is almost double that corresponding to shear cracking.

Introduction

Knowledge of the mixed mode fracture of concrete materials with the effect of impact loading is essential to predict the failure mechanisms in concrete structures(1). In general, the fracture of reinforced concrete elements occurs under combined mode I and mode II loading conditions(2). Little information is available on fracture properties of concrete subjected to combined tensile and shear stresses with the effect of loading rate.

As far as mixed mode fracture is concerned, various specimen and test configurations can be used, as shown in Fig. 1. By introducing a central notch on a disk specimen, mixed mode fracture conditions can be obtained with a wide range of proportions between the tensile and shear components. Figure 2 shows how it is possible by rotating the notch inclination angle β with respect to the loading direction to change the mode of fracture from tensile (mode I for $\beta = 0°$) to mixed mode (tension-shear for $\beta < 30°$ and compression-shear for $\beta > 30°$)(3).

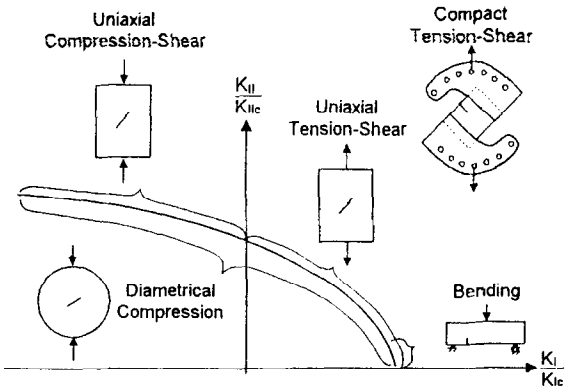

FIG. 1.
Different loading configurations for test of mixed mode fracture.

The study presented in this paper includes testing of center notched disk specimens with different notch inclination angles at different rates of loading. First, a quasi-static rate of loading was used under closed loop conditions. Both holographic interferometry and reflection photoelasticity with conventional TV imaging (30 frames per second) were used to observe the mixed mode fracture processes of the specimens. Laser holographic interferometry was used to evaluate and calibrate the photoelastic measurements to ensure that the photoelasticity can be applied in the tests at higher rates. For higher rates of loading, a modified Charpy machine and high speed photography (10,000 frames per second) with reflection photoelasticity were used.

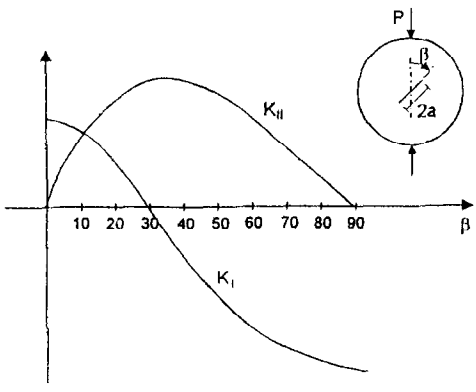

FIG. 2.
Variation of stress intensity factors for CND specimen.

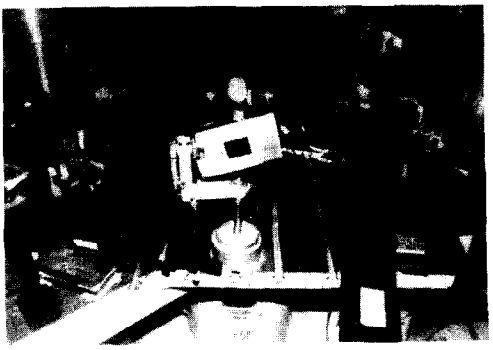

FIG. 3.
Loading frame and laser optics.

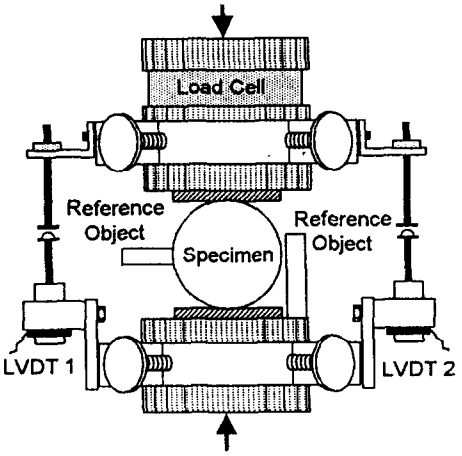

FIG. 4.
Specimen setup for quasi-static loading test.

Testing Procedure

Quasi-Static Loading. Center notched disk specimens were used. The mortar used to cast the specimens had mix-proportions of 1.0/2.0/0.5 (cement/sand/water) by weight. Center notched cylinders of dimension 50.8mm × 57.2mm with a 9.5mm central notch were cast first and then polished down to 50.8mm long to obtain smooth and parallel surfaces. After casting, the specimens were cured in lime saturated water until needed. The specimens were loaded diametrically (Brazilian test) using a 535.2 kN capacity loading frame (Fig. 3) with a closed

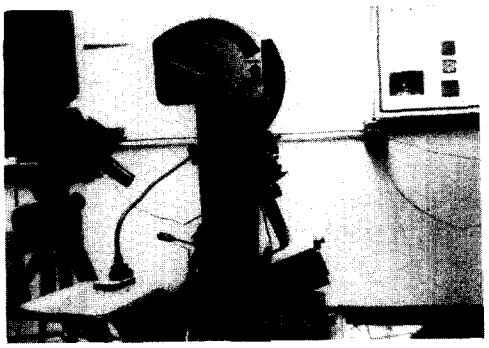

FIG. 5.
Charpy machine for impact loading tests.

FIG. 6.
Charpy machine striker-support assembly.

loop hydraulic system. As shown in Fig. 4, a specimen was placed between the loading platens. A dual LVDT transducer was used to measure axial displacement while the applied load was measured using a cylindrical load cell transducer. The specimens were tested up to the limit of the instrumentation used for closed loop control.

Holographic interferometry was used primarily at the quasi-static rate of loading because its accuracy and sensitivity can reach a sub-micron range in displacement measurement. An optical setup for three dimensional holographic interferometry was arranged around the test specimen on the loading frame. The feedback control system of the loading frame was redesigned to be so accurate and stable that sandwich holograms(4)(5) can be made on the loading frame without any vibration isolation. Real-time holographic interferometry was used to monitor and control the loading increments. Figure 3 shows the laser optics arranged on the loading frame. The details of the laser holographic test are given in a separate paper(6).

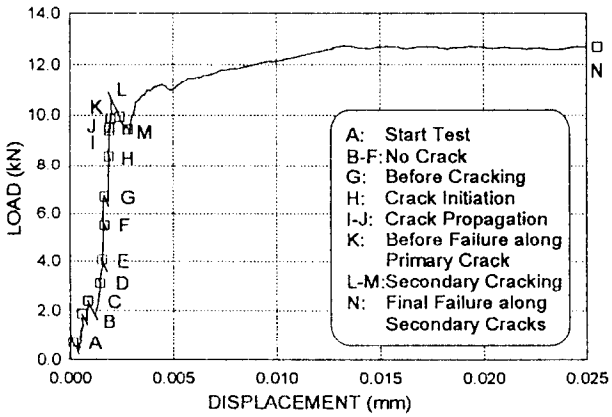

FIG. 7.
Holographic test at quasi-static rate ($\beta = 0°$).

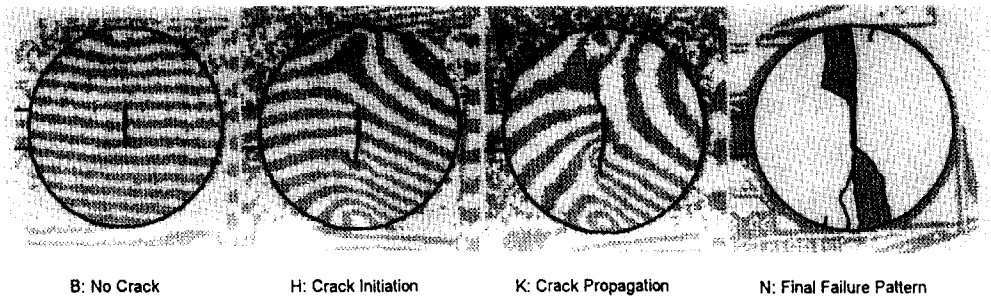

FIG. 8.
Holographic interferometric fringe patterns ($\beta = 0°$).

For the photoelastic test, a coating of type PS-1, 0.25mm thick, was glued to each surface of a test specimen to preserve symmetry. A reflection polariscope of model 030 (Measurements Group) was used to produce isochromatic fringe patterns. A Panasonic S-VHS TV camera was used to record the isochromatic fringes continuously.

Instrumented Impact Loading. Figure 5 shows the experiment arrangement for the impact loading tests. The instrumented Charpy machine used by Gopalaratnam(7)(8) was modified to accommodate center notched disk specimens. A modified instrumented striker (tup), an instrumented anvil, a specimen support and an anchor were fabricated. Figure 6 shows the general assembly for the modified Charpy machine. Full Wheatstone bridge circuits were connected on both tup and anvil. They were sensitive only to axial load. A Tektronix 2232 model oscilloscope was used for data acquisition at a rate of 250 KHz. Both the striker and the anvil were calibrated at static rate of loading in a 89.2 kN capacity loading frame up to 44.6 kN under load control mode. Dynamic calibration was achieved by placing a dynamic load cell transducer in place of the specimen. In order to estimate the inertial effect dummy specimens

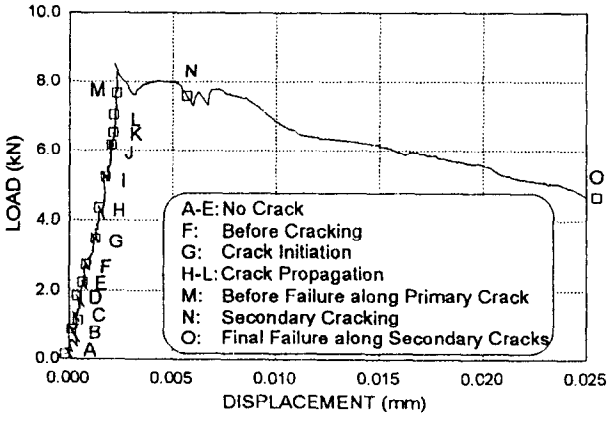

FIG. 9.
Holographic test at quasi-static rate ($\beta = 54°$).

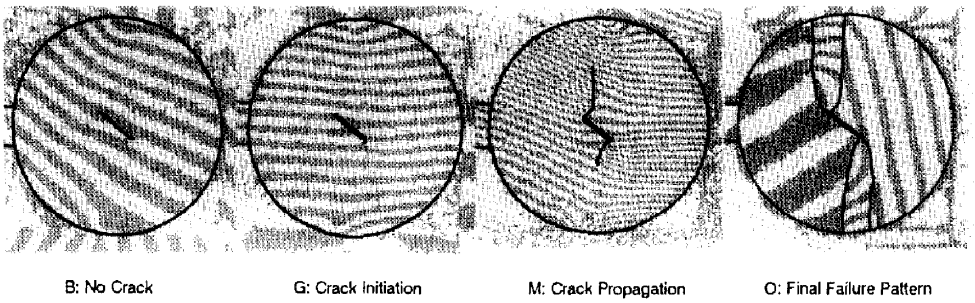

FIG. 10.
Holographic interferometric fringe patterns ($\beta = 54°$).

were tested and the responses from the tup and anvil were compared. It was found that both peak load and arrival time differences are small (5 percent) compared to the overall response so that the inertial effect can be neglected.

For evaluation of crack propagation, the same photoelastic coating as in quasi-static loading tests was glued to both front and back faces of specimens. A lens was incorporated in the polariscope setup to increase the light intensity to the level required for high speed photography. Halogen light was used for illumination. A high speed motion picture camera of model 100 (Photographic Analysis Company) was used for recording of isochromatic fringes. Films of Kodak SO-259 (400 ASA, 137 m rolls) for high speed photography were used. The high speed camera was used to trigger the overall system. After a time delay required to bring the film up to speed, the camera closed an electric circuit which activated a relay to release the pendulum of the Charpy machine. Data acquisition was triggered by the impact between the striker and the specimen. A second Tektronix 2232 model oscilloscope was used at low frequency (5 KHz) to measure the time difference between the release of the pendulum and impact with the specimen.

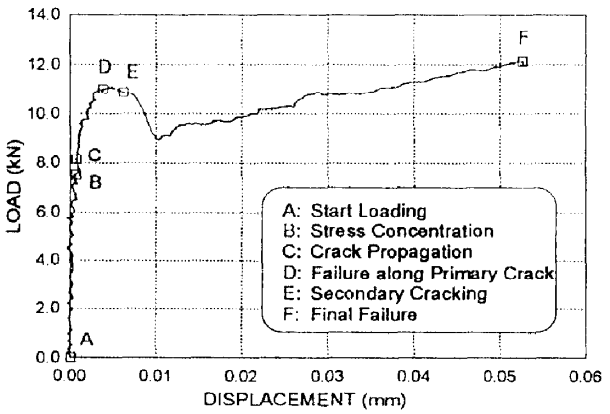

FIG. 11.
Photoelastic test at quasi-static rate ($\beta = 0°$).

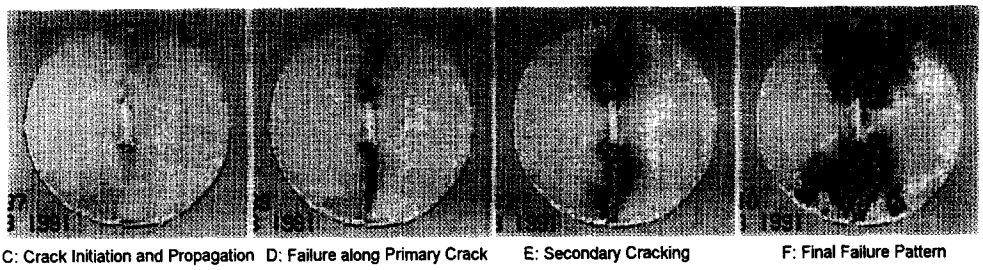

FIG. 12.
Isochromatic fringe patterns at quasi-static rate ($\beta = 0°$).

Results

Quasi-Static Loading with Holographic Interferometry. Specimens were tested at five different notch inclination angles (0°, 18°, 36°, 54° and 72°). The test result of a 0° notched specimen using holographic interferometry is characterized in Fig. 7 and Fig. 8. The load-displacement curve in Fig. 7 has the same shape as that reported by Ojdrovic(9). The fracture process of the specimen was observed from the holographic recordings which are marked with squares on the curve and labeled from A to N in Fig. 7. The test started at the point A and the first step of double exposure holographic interferometry was made at point B. The crack initiation from the bottom notch tip was captured first at point H and then the primary crack propagated up and down. Stable crack growth occurred after point H even though there was no macroscopic evidence of nonlinearity. At point K, the crack had gone partly through the height of the specimen. After point K, this primary crack went through the specimen (points L and M). Further increase of load after this point was possible, as a result of friction at the loading points. When the loading sequence was completed, at point N, a second set of cracks starting from the perimeter of the cylinder had formed, initiating the wedge formation reported by Ojdrovic(9). Figure 8 shows the particular holographic recordings at points B, H, K and N.

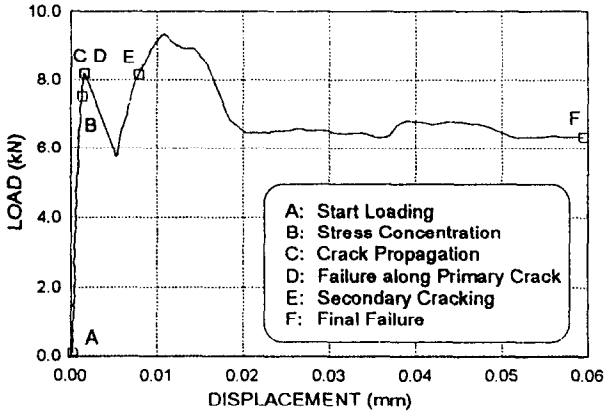

FIG. 13.
Photoelastic test at quasi-static rate ($\beta = 54°$).

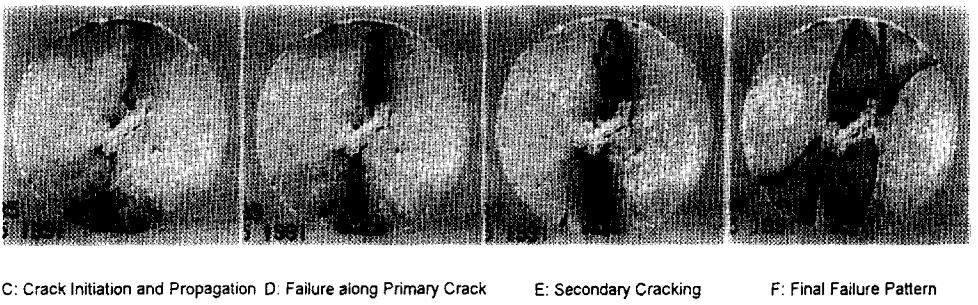

FIG. 14.
Isochromatic fringe patterns at quasi-static rate ($\beta = 54°$).

The load-displacement curve for a 54° notched specimen is shown in Fig. 9. The points of holographic recordings are labeled from A to O. The descending part of the curve immediately after unstable crack propagation indicates a reduction of the ductility as compared to the 0° case. Stable crack growth was still possible and occurred between points G and M. Signs of secondary cracking were also found at the completion of the experiment, Point O. Interferometric fringe recordings at points B, G, M and O are shown in Fig. 10. In general, similar conclusions to those from the 0° notched specimens can be made. After the primary crack initiated at the bottom notch tip, the upper crack propagated slightly faster than the bottom one. The primary cracks propagated in a stable manner up to the peak load.

It should be mentioned that due to its sub-micron range of accuracy and sensitivity in displacement measurement, the holographic interferometry is sensitive enough to detect cracks in their early stages(6).

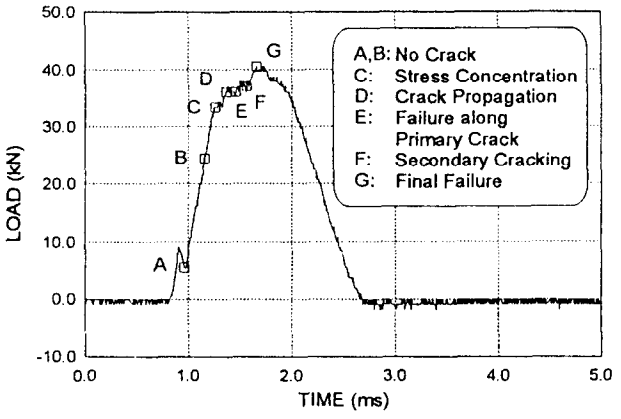

Fig. 15.
Photoelastic test at impact rate ($\beta = 0°$).

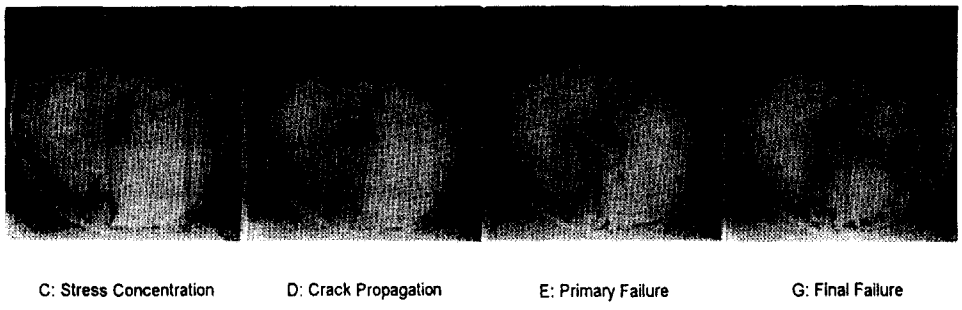

FIG. 16.
Isochromatic fringe patterns at impact rate ($\beta = 0°$).

Quasi-Static Loading with Reflection Photoelasticity. The results of photoelastic tests with two of the five notch inclination angles are given in the following paragraphs. Both the load-displacement curves and the overall crack growth patterns agree with the observation obtained by using laser holographic interferometry.

Figure 11 shows the load-displacement curve for a specimen with vertical notch inclination $\beta = 0°$ tested under photoelasticity. Continuous imaging at a video rate of 30 images per second were recorded using a S-VHS video tape recorder. The most significant stages of crack propagation are marked as squares on the curve and labeled from A to F in Fig. 11. Note that this curve is similar to the one in the holographic test. Some of the key photographic recordings are shown in Fig. 12. The first crack initiation and propagation happened at point C and the primary crack grew through the height of the specimen at point D. The crack initiation detected by photoelasticity occurred at a higher load level compared to the laser holography. After failure along the primary crack, the load kept increasing until secondary cracks initiated at point E from the left side of the top end. The secondary failure mechanism resulted in failure wedges, as shown at point F in Fig. 12. However, even after large crack openings, the photoelastic coating provided a relatively strong support at the crack faces.

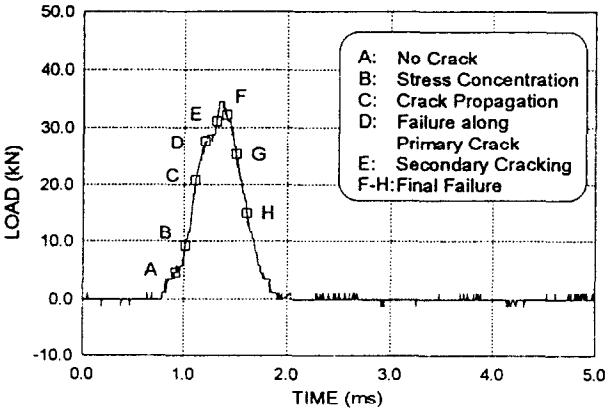

FIG. 17.
Photoelastic test at impact rate ($\beta = 54°$).

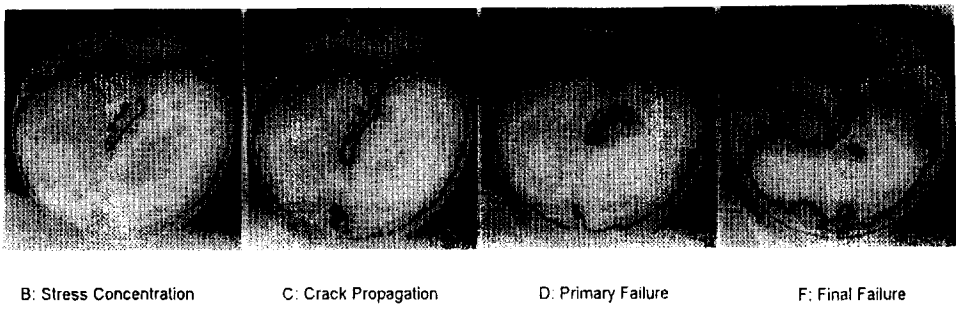

FIG. 18.
Isochromatic fringe patterns at impact rate ($\beta = 54°$).

Figures 13 and 14 show the load-displacement curve and isochromatic fringe patterns for a specimen with notch inclination angle $\beta = 54°$. The primary crack initiated and propagated very fast through the specimen height between points C and D located before the first peak of the load-displacement curve. No stable crack growth was detected with photoelasticity as it was with holography. The second peak reached a slightly higher load value than the first one. The top of the second peak can be correlated to the initiation of the secondary crack at point E from the left side of the bottom end. Between the two peaks the physical mechanism was characterized by opening of the primary crack and the reinforcing effect of the photoelastic coating becomes evident. After the secondary cracks had grown, there was a plateau in the load-displacement curve while collapse of the specimen occurred at point F after the photoelastic coating had debonded from the specimen.

Post-failure examination of tested specimens indicated that the concentration of isochromatic fringes followed closely the crack trajectory on the surface of the specimen. Thus, the possibility of local debonding of the photoelastic coating before cracking should be eliminated.

In general, an acceptable agreement was found between holographic and photoelastic observations regarding crack formation and propagation at slow rate of loading. The modes

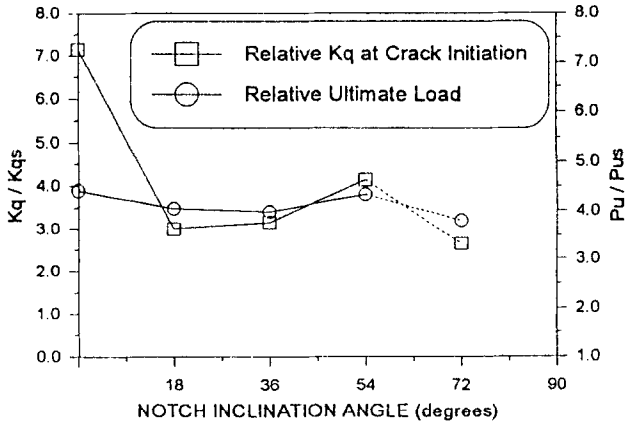

FIG. 19.
Relative apparent stress intensity factor ($K_q/K_{qstatic}$).

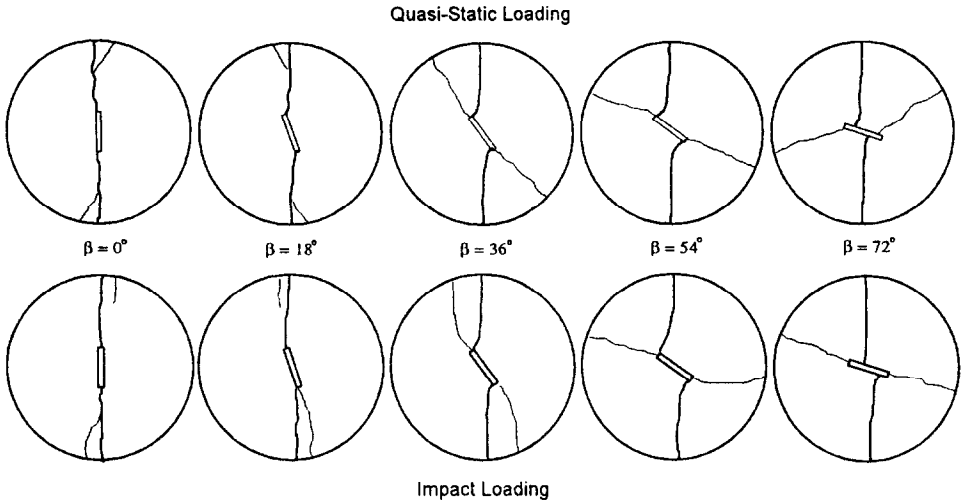

FIG. 20.
Failure modes at quasi-static and impact loading.

of failure were not modified by the existence of the photoelastic coating and, although some reinforcing effects were observed, the structural behavior of the specimens showed the same trends for different notch inclination angles. Also, the sensitivity with photoelasticity is lower than that observed with the laser holography. For example, crack initiation was not detected prior to peak load for some specimens even though holographic measurements indicated a significant stage of crack growth. Therefore, the reflection photoelasticity can only be used to determine qualitatively the patterns of crack growth.

Impact Loading with Reflection Photoelasticity. The impact energy was selected such that the failure mode remained the same as that observed during the slow rate experiments. Therefore, the observed macroscopic rate effects can be related only to the rate effect on crack initiation and crack growth. Much higher rates of loading than used here usually result in fragmentation of the specimens and different failure mechanisms.

Figure 15 shows the recorded load signal for the specimen with notch inclination angle $\beta = 0°$. Each isochromatic fringe pattern was recorded at constant intervals of 0.1 ms. However, the timing of the photographic exposures can only be determined within 0.05 ms (i.e. photographic exposures could be shifted forward or backward by 0.05 ms in Fig. 15 but the interval between exposures remains 0.1 ms). Figure 16 shows the sequence of isochromatic fringe pattern recordings corresponding to the same specimen. Unfortunately, the pictures shown in this paper are not as clear as the original film due to the reproduction process but some observation can still be made. The failure sequence agreed with the holographic and photoelastic observations at low rate of loading. At point C, it showed a concentration of stress along the crack path but it was unclear whether a crack had initiated or not. At point D, there was a crack on each tip of

the notch and they started to propagate up and down. At point E, the primary crack had propagated through the specimen. There was what appeared to be an unloading region in the load-time curve at point E. This corresponded to the first peak observed at low rate of loading. A second peak was found at point G where the secondary cracks initiated and propagated. Post-failure examination of the specimens showed that the crack patterns corresponded to the holographic and isochromatic fringe patterns. Debonding of the photoelastic coating was also observed. Further examination of the failed specimens showed that debonding occurred between the photoelastic coating and the reflecting paint on the back face of the photoelastic medium.

The load signal for a specimen with notch inclination angle $\beta = 54°$ is shown in Fig. 17. Figure 18 shows the sequence of isochromatic fringe pattern recordings corresponding to this specimen. The isochromatic fringe pattern at point B showed a concentration of stress around both notch tips. The crack initiation and propagation were detected at point C. At point D, the primary crack had propagated to the perimeter of the specimen. The final failure was accompanied by formation of secondary cracks and debonding of the photoelastic coating at point F.

In general, for all the specimens studied it was found that crack initiation and growth can be correlated to the state of loading of the specimens. There was no apparent retardation of the crack growth compared to the loading sequence. Thus, it can be concluded that for the rates of loading used during this investigation failure was characterized by stable crack growth. Crack propagation velocity at this load rate appeared to be more a function of the applied load than a material property.

Figure 19 shows the relative apparent stress intensity factor K_q for different notch inclination angles. Note that the comparison should be made at crack initiation since after the crack propagation it becomes a tension crack for all notch inclinations. From this figure it can be concluded that the increase in apparent fracture toughness for a tension crack ($\beta = 0°$) was higher than that for a shear crack ($\beta = 36°$). Also, note that between notch inclination angles $\beta = 18°$ and $36°$ the relative K_q was minimum, which corresponds to the maximum shear component. In Fig. 19 the values corresponding to $\beta = 72°$ should not be considered very reliable because the cracks did not start from the notch tips as expected.

Fig. 20 gives a summary of failure modes for both quasi-static and impact rates of loading at various notch inclination angles. Note that for the rates of loading used during this investigation the failure modes remain essentially the same. Thus, any variation in the macroscopic response should be related to change in fracture toughness.

Conclusions

(1) Reflection photoelasticity can be used to determine crack initiation and crack growth at both quasi-static and impact rates of loading. However, it is not sensitive enough to provide information regarding the state of deformation away from the crack path.

(2) The reinforcing effect of the photoelastic coating is evident in the post-peak region but it is not large enough to modify the failure mode.

(3) There was good agreement at quasi-static loading between the observations made using holographic interferometry and reflection photoelasticity regarding crack initiation, crack growth and failure mechanisms.

(4) At both quasi-static and impact loading, the state of cracking can be correlated to the

loading stage of the specimens. For all notch inclination angles, there are three loading regions limited by crack growth, crack opening and secondary cracking. At the rates of loading used during this investigation, failure appears to be characterized by stable crack growth.

(5) The increase in fracture toughness at high rates of loading is affected by the mode of fracture. The increase of fracture toughness for tensile cracking is approximately double the corresponding to mode II cracking.

Acknowledgment

This study was made possible through the support of the Department of the Air Force of the United States (Contract No. C-F08635-89-C-0182).

References

1. C.T. Yu, A.S. Kobayashi and N.M. Hawkins, Journal of Experimental Mechanics, 33(3), 205-211 (1993).
2. A.K. Maji, M.A. Tasdemir and S.P. Shah, Engineering Fracture Mechanics, 38(2/3), 129-145 (1991).
3. C. Atkinson, R.E. Smelser and J. Sanchez, International Journal of Fracture, 18(4), 279-291 (1982).
4. N. Abramson, The Making and Evaluation of Holograms, Academic Press, 97-108 (1981).
5. R.A. Miller, S.P. Shah and H.I. Bjelkhagen, Journal of Experimental Mechanics, 28(4), 388-394 (1988).
6. A. Castro-Montero, Z. Jia and S.P. Shah, ACI Materials Journal, to be published.
7. V.S. Gopalaratnam, S.P. Shah and R. John, Journal of Experimental Mechanics, 24(2), 102-111 (1984).
8. V.S. Gopalaratnam and S.P. Shah, ACI Materials Journal, 83(8), 117-126 (1985).
9. R.P. Ojdrovic and H.J. Petroski, Journal of Engineering Mechanics, 113(12), 1551-1564 (1987).